Received: 11 July 2018 | Revised: 19 November 2018 | Accepted: 24 November 2018

DOI: 10.1111/cbdd.13459

WILEY C&B DRUG DESIGN

RESEARCH ARTICLE

Synthesis and biological evaluation of quinoxaline derivatives as tubulin polymerization inhibitors that elevate intracellular ROS and triggers apoptosis via mitochondrial pathway

Jianguo Qi[1] | **Jing Huang**[1] | **Xiaomin Zhou**[1] | **Wen Luo**[1] | **Jiaxin Xie**[1] | **Linqiang Niu**[1] | **Zhijie Yan**[1] | **Yang Luo**[1] | **Yuhui Men**[1] | **Yanan Chen**[2] | **Yahong Zhang**[1] | **Jianhong Wang**[1]

[1]Key Laboratory of Natural Medicine and Immuno-Engineering of Henan Province, Henan University Jinming Campus, Kaifeng, Henan, China

[2]Institute of Behavior and Psychology, Henan University Jimming Campus, Kaifeng, Henan, China

Correspondence
Yahong Zhang and Jianhong Wang, Key Laboratory of Natural Medicine and Immuno-Engineering of Henan Province, Henan University Jinming Campus, Kaifeng, Henan, China.
Emails: zhangyahong_131@163.com and jhworg@126.com

Funding information
Program for Science Technology Innovation Talents in Universities of Henan Province, Grant/Award Number: 16HASTIT029; Key Scientific Research Program of the Higher Education Institutions of Henan Province, Grant/Award Number: 15A350005; National Natural Science Foundation of China, Grant/Award Number: 21272056, U1704176 and U1404819; Henan University, Grant/Award Number: 2015YBZR043

Abstract

A series of novel quinoxaline derivatives were synthesized and evaluated for their antiproliferative activity in three human cancer cell lines. Compound **12** exhibited the most potent antiproliferative activity with IC_{50} in the range of 0.19–0.51 μM. The compound inhibited tubulin polymerization and disrupted the microtubule network, leading to G2/M phase arrest. Furthermore, compound **12** induced ROS production and malfunction of mitochondrial membrane potential. Compound **12** led to cancer cells apoptosis in a dose-dependent manner. Western blot analysis showed that compound **12** induced up-regulation of p21 and affected the expression of cell cycle-related proteins. The binding mode was also probed by molecular docking.

KEYWORDS

cell apoptosis, G2/M phase arrest, quinoxaline derivatives, reactive oxygen species, tubulin polymerization inhibitors

1 | INTRODUCTION

Microtubules, which are dynamic polymers of α/β-tubulin, are elements of the cellular cytoskeleton and involved in numerous cellular functions such as cell movement, organelle localization, and cell division. Microtubules have been considered an ideal target for cancer chemotherapy because of the important role they play in mitosis. There are four well-characterized sites for microtubule-disrupting agents (MDAs) in tubulin: taxanes, vinca alkaloids, laulimalide, and colchicine (Bhalla, 2003; Dumontet & Jordan, 2010; Jordan & Wilson, 2004). Currently, all the United States Food and Drug Administration (FDA) approved MDAs for cancer therapy target either taxanes (e.g., paclitaxel, docetaxel) or vinca alkaloids (e.g., vinblastine, vincristine). However, the clinical efficacy of the drugs is often limited by occurrence and evolution of resistance mechanisms that is further compounded by a narrow therapeutic index (Du et al., 2015; Gigant et al.,

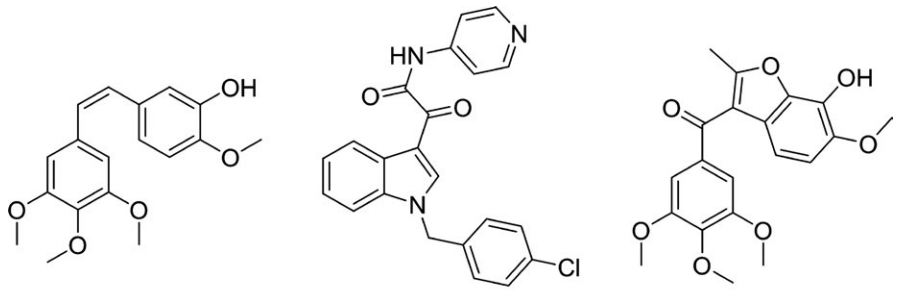

1 (Combretastatin A4) **2** (Indibulin) **3** (BNC-105)

FIGURE 1 Microtubule-disrupting agents inhibiting tubulin polymerization

2005; Kavallaris, 2010; Perez, 2009; Wang, Chen, Miller, & Li, 2014; Wang et al., 2012). Recently, some colchicine binding tubulin inhibitors exhibit significant ability to overcome multidrug resistance (Bacher et al., 2001; Banerjee et al., 2018; Bueno et al., 2018; Cui et al., 2017; Dohle et al., 2018; Gangjee et al., 2010; Lauria et al., 2018; Li et al., 2018; Ohsumi et al., 1998; Pang et al., 2017; Suman et al., 2015). Even some drug candidates have already entered the clinical trial stage (Figure 1). However, the potential clinical applications of tubulin inhibitors have been restricted by low solubility, low bioavailability, and lack of tumor selectivity (Lu, Chen, Xiao, Li, & Miller, 2012; Stanton, Gernert, Nettles, & Aneja, 2011). Therefore, there are ongoing research efforts to identify novel scaffolds that target the site of colchicine binding that display improved physicochemical properties and selectivity toward cancer cells.

Reactive oxygen species (ROS), oxygen-free radicals produced in biological systems, play an important role in chemotherapy. High intrinsic levels of ROS and up-regulation of cellular antioxidant machinery are defining changes in tumor cells exhibiting glycolysis(Szatrowski & Nathan, 1991). In general, the mechanisms by which antioxidants are produces in the body are performing at maximum capacity due to a higher basal level of ROS. By taking advantage of this fact, chemical agents that cause additional oxidative stress results in cancer cells that are more vulnerable to small molecule chemotherapy, thus providing a mechanism for selective targeting of cancer cells (Asby et al., 2016; Hirota et al., 1999; Huang, Feng, Oldham, Keating, & Plunkett, 2000; Lecane et al., 2005; Raj et al., 2011).

Quinoxaline, present in many bioactive compounds, displays adequate physicochemical properties and drug-like properties (Ajani, 2014; Tariq, Somakala, & Amir, 2018). Numerous synthetic quinoxaline derivatives have shown interesting antineoplastic activity. For instance, the substitution of the benzene ring by quinoxaline in Combretastatin-A4 improved both the physicochemical properties and biological activity (Pérez-Melero et al., 2004). The novel fusion of 3,4-dihydroquinoxalin-2(1*H*)-one with 2*H*-isoindole results in a series of compounds which showed dual inhibition of tubulin polymerization and topoisomerase I (Diana et al., 2008). Previously, we have synthesized a series of 3,4-dihydroquinoxalin-2(1*H*)-one derivatives targeting the colchicine binding site on tubulin (Qi et al., 2018).

The series of quinoxaline derivatives include many scaffolds, such as quinoxaline, 3,4-dihydroquinoxa lin-2(1*H*)-one, quinoxaline-2,3(1*H*,4*H*)-dione, and 1,2,3,4-tetrahydroquinoxaline. Based on the previous research, the 3,4-dihydroquinoxalin-2(1*H*)-one scaffold was replaced with quinoxaline-2,3(1*H*,4*H*)-dione or 1,2,3,4-tetrahydroquinoxaline scaffold. Herein, we report the synthesis and biological evaluation of quinoxaline-2,3(1*H*,4*H*)-dione and 1,2,3,4-tetrahydroquinoxaline scaffolds derivatives to develop tubulin polymerization inhibitors as antitumor agents (Figure 2).

2 | METHODS AND MATERIALS

2.1 | Chemistry

All commercially obtained reagents and solvents were used as received. HRMS spectra were acquired on a Thermo Scientific LTQ Orbitrap XL mass spectrometer, and all the errors were <3 ppm. ^{1}H NMR spectra, and ^{13}C NMR spectra were acquired on a Bruker DRX 300 NMR spectrometer using $CDCl_3$ or DMSO-d_6 as solvent (unless otherwise stated). Chemical shifts were reported in parts per million (ppm, δ) relative to the solvent peak (^{1}H, $CDCl_3$ δ 7.26 ppm, DMSO-d_6 δ 2.50 ppm; ^{13}C, $CDCl_3$ δ 77.0 ppm, DMSO-d_6 δ 39.5 ppm). Coupling constants (*J*) were measured in hertz (Hz). The synthesis and chemical characterization of the compounds are in the Supporting Information Table S1.

2.2 | Biological evaluation

2.2.1 | Cell lines and culture conditions

The human epithelial cervical cancer cell line HeLa, the human hepatoma cell line SMMC-7721, and the human intestinal epithelial cell line HT-29 were cultured in RPMI

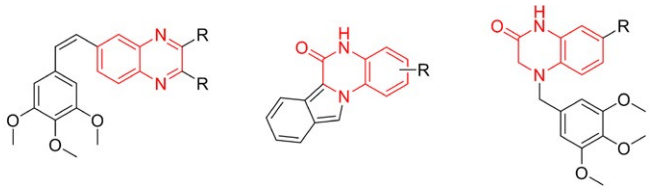

FIGURE 2 Quinoxaline derivatives and different quinoxaline scaffolds

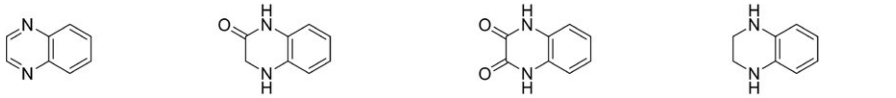

1640 medium (HyClone Co., USA), supplemented with 10% fetal bovine serum (Sijiqing Biotechnology Co., China), in 5% CO_2 humidified air at 37°C. All the cell lines were obtained from the American Type Culture Collection (ATCC, USA).

2.2.2 | In vitro antiproliferative activity

The MTT assay was used to determine the antiproliferative effects of the synthesized compounds. Cells were seeded into 96-well plates with the density of 4,000–6,000 cells per well. After 24 hr of growth to allow attachment of cells to the well, test compounds were added at five different concentrations. After incubation for 72 hr, 50 µl of MTT solution (10 mg/ml in PBS) was added. After 4 hr of incubation in the dark, the medium was removed and replaced with 100 µM DMSO. After shaking for 10 min, the optical density was measured at a wavelength of 490 nm using a microplate reader (Powerwave XS, Biotek, USA). Experiments were performed in triplicate and repeated at least three times.

2.2.3 | Tubulin polymerization assay

Tubulin polymerization assay was conducted using a fluorescence-based tubulin polymerization assay kit (BK011P, Cytoskeleton, USA) according to the manufacturer's protocol. The final reaction mixture contained 2 mg/ml tubulin, 2.0 mM $MgCl_2$, 0.5 mM EGTA, 1.0 mM GTP, 15% glycerol, 80 mM PIPES, and test compound. The fluorescence intensity was measured for 1 hr at 1 min intervals in CLARIOstar microplate reader (BMG Labtech Inc., Germany). Experiments were performed in duplicate.

2.2.4 | Immunofluorescence microscopy

HeLa cells were seeded in a 96-well plate at 4,000 cells per well and incubated for 24 hr. Then, the cells were treated with vehicle or different concentrations of test compound. After incubation for 24 hr, cells were fixed in 4% paraformaldehyde for 10 min at 4°C and permeabilized with 0.1% Triton X-100 in PBS for 5 min at 4°C. After then, the cells were processed for immunofluorescence with the primary antibody (Catalog No. BM1452, Boster Co. Ltd., China, 1:100 dilution in 2% BSA-PBS) and anti-mouse secondary antibody conjugated with FITC for 30 min at 37°C (Catalog No. BA1101, Boster Co. Ltd., China, 1: 100 dilution in 1% BSA-PBS) separately. The nuclei were stained with Hoechst 33342, and immunofluorescence was detected using a fluorescence microscope (Leica TCS SP8, Germany).

2.2.5 | Flow cytometric analysis of cell cycle and apoptosis

Cell cycle distribution was analyzed after incubation with PI, and apoptosis was analyzed after staining with annexin V-FITC in combination with PI. The samples were analyzed using the flow cytometer (BD FACSVerse, USA).

2.2.6 | ROS production

HeLa cells were treated with vehicle or different concentrations of the test compound for 24 hr. Then, the cells were treated with ROS indicator DHE (Beyotime Biotechnology Co. Ltd., China). The cells were detected using the fluorescence microscope or analyzed by the flow cytometer described above.

2.2.7 | Measurement of mitochondrial membrane potential

HeLa cells were treated with vehicle or different concentrations of the test compound for 24 hr. Then, the cells were incubated with the mitochondrial membrane potential probe (JC-1, Beyotime Biotechnology Co. Ltd., China) for 30 min. The cells were detected using the fluorescence microscope or analyzed by the flow cytometer described above.

2.2.8 | Western blot analysis

HeLa cells were incubated with vehicle or different concentrations of the test compound for 24 hr. Then, the cells were

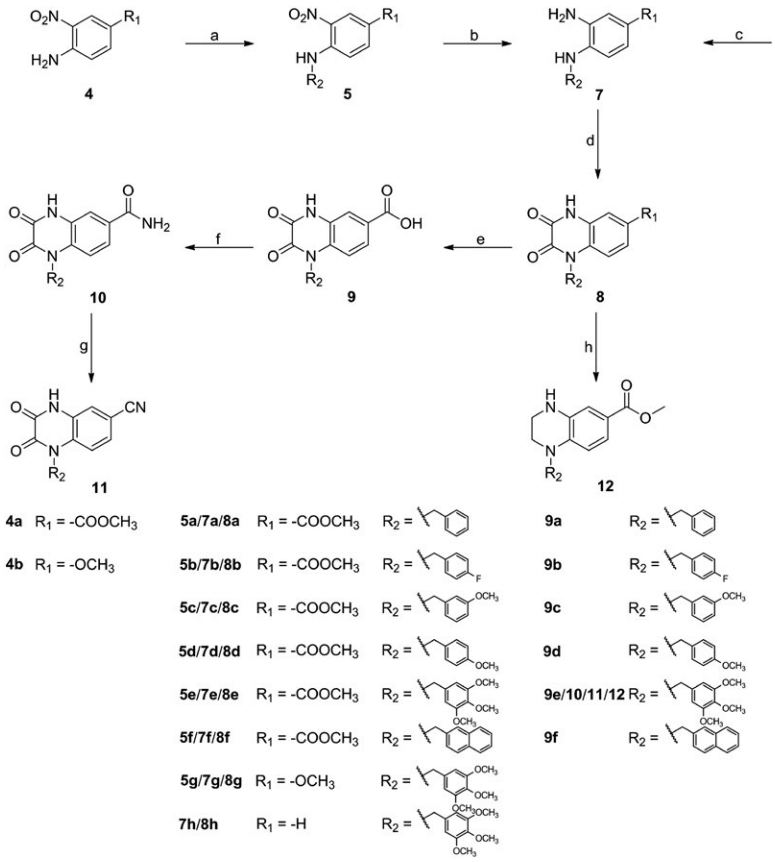

SCHEME 1 Reagents and conditions: a) benzyl chlorides, KI, K_2CO_3, CH_3CN, 70°C; b) 10% Pd/C, H_2, MeOH, rt; c) 3,4,5-trimethoxybenzyl chloride, KI, K_2CO_3, CH_3CN, 70°C; d) dimethyl oxalate, 140°C; e) NaOH, THF, H_2O, rt; f) Boc anhydride, ammonium bicarbonate, pyridine, 1,4-dioxane, rt; g) phosphorus oxychloride, $CHCl_3$, reflux; h) borane, THF, rt

collected, centrifuged, and washed with ice-cold phosphate-buffered saline (PBS). The pellet was resuspended in lysis buffer and incubated on ice for 30 min, and then the lysates were centrifuged at 15,000 *g* at 4°C for 10 min. The protein concentration was determined using the Bio-Rad protein assay (Bio-Rad Laboratories, Mississauga, Canada). Equal amounts of protein were analyzed by SDS-PAGE and then transferred to PVDF membrane. Membranes were blocked with a 5% bovine serum albumin solution and then incubated with the specific primary antibodies. After washing, the membrane was incubated with peroxidase-conjugated secondary antibodies for 1 hr.

2.3 | Molecular modeling

The docking study was carried out using SYBYL-X 2.1. The crystal structure of tubulin in complex with DAMA-colchicine was retrieved from PDB (1SA0). The 3D structure of **12** was built using SYBYL-X 2.1 and minimized using tripos force field and Gasteiger–Huckel charges. Powell's method was employed with gradient convergence criteria of 0.005 kcal/mol. The DAMA-colchicine structure was extracted, and the tubulin structure was prepared and minimized with Amber7 F99 force field. The binding site was constructed by the ligand protomol of surflex dock. Compound **12** was docked into the DAMA-colchicine binding site.

3 | RESULTS AND DISCUSSION

3.1 | Chemistry

The synthesis of the compounds was depicted in Scheme 1. Reaction of compound **4** with substituted benzyl chloride provided intermediate **5** which upon further reduction yielded intermediate **7**, except for **7h**, which was prepared by the reaction of o-phenylenediamine (**6**) with 3,4,5-trimethoxybenzyl chloride. Compound **8** was prepared by reaction of intermediate **7** with dimethyl oxalate. Hydrolysis of compound **8** afforded compound **9.** Compound **10** was synthesized by the reaction of compound **9e** with ammonium bicarbonate. Compound **11** was prepared by dehydration of compound **10**. Reduction of compound **8e** provided compound **12**.

3.2 | Biological evaluation

3.2.1 | In vitro antiproliferative activity

The antiproliferative activities of the synthesized target compounds were evaluated against three distinct human cancer cell lines, including HeLa (human epithelial cervical cancer), SMMC-7721(human hepatoma cancer), and HT29 (human intestinal epithelial cancer) cell lines using an MTT assay. Indibulin, the tubulin inhibitor that was explored in clinical trials for cancer therapy was used as reference compound.

The results are summarized in Table 1. The antiproliferative activities of the compounds were expressed as the concentration of compounds required for 50% growth inhibition of the cells (IC_{50}). IC_{50} values were calculated from at least five different concentrations of test compounds.

As shown in Table 1, the comparison of antiproliferative activities of **8a**–**8f** demonstrated that 3,4,5-trimethoxybenzyl substitution on the nitrogen atom of methyl 2,3-oxo-1,2,3,4-tetrahydroquinoxaline-6-carboxylate (**8e**) showed improved activity. When the methyl carboxylate (**8a**–**8f**) was hydrolyzed to carboxylic acid (**9a**–**9f**), the antiproliferative activities decreased. Compound **8g** exhibited better activities than **8e**, **8h**, **10**, and **11**, indicating that 6-methoxy exhibited better activity than 6-carboxylate, 6-H, 6-carboxamide, and 6-carbonitrile in the substituted 2,3-oxo-1,2,3,4-tetrahydroquinoxaline. Compound **12**, the reduction product of **8e**, showed potent antiproliferative activities. It exhibited better activity than indibulin. This indicated that 1,2,3,4-tetrahydroquinoxaline was a privileged scaffold, and compound **12** could potentially be a novel lead structure for further extensive optimization.

TABLE 1 The in vitro antiproliferative activities of synthesized target compounds (**8a**–**8h**, **9a**–**9f**, **10**, **11**, **12**) doxorubicin and indibulin against three human cancer cell lines (HeLa, SMMC-7721 and HT29)

	Antiproliferative activity IC_{50} (μM)		
Compound	**HeLa**	**SMMC-7721**	**HT29**
8a	>50	43.5 ± 4.5	43.7 ± 5.9
8b	33.3 ± 7.8	39.6 ± 4.8	40.2 ± 5.1
8c	35.1 ± 6.1	34.7 ± 2.6	47.2 ± 5.5
8d	15.3 ± 4.1	43.4 ± 2.1	15.0 ± 1.2
8e	3.42 ± 1.02	8.02 ± 0.62	3.71 ± 0.26
8f	29.9 ± 4.7	34.3 ± 3.3	38.4 ± 7.6
8g	0.693 ± 0.185	1.60 ± 0.37	1.48 ± 0.22
8h	28.1 ± 2.4	28.8 ± 3.4	23.0 ± 1.5
9a	45.6 ± 8.0	46.2 ± 2.7	49.0 ± 4.3
9b	>50	>50	>50
9c	42.8 ± 7.9	>50	38.2 ± 2.3
9d	39.0 ± 5.9	38.4 ± 1.4	47.9 ± 4.2
9e	34.1 ± 5.6	>50	>50
9f	>50	>50	>50
10	39.6 ± 5.5	38.1 ± 1.7	45.2 ± 2.4
11	>50	>50	>50
12	0.194 ± 0.013	0.427 ± 0.054	0.510 ± 0.036
Indibulin	0.532 ± 0.055	0.621 ± 0.058	0.633 ± 0.081

3.2.2 | Effects on tubulin polymerization

Microtubules are crucial components of mitotic spindle in the process of mitosis, and as such has become an important target for cancer therapy. Most microtubule-targeted antitumor agents either stabilize or destabilize tubulin polymerization. In this study, a tubulin polymerization assay was performed to confirm the interference of compound **12** in tubulin polymerization. As shown in Figure 3, the fluorescence intensity increased gradually when the purified and unpolymerized tubulin was incubated at 37°C and this demonstrated that tubulin polymerization had occurred (control sample). When tubulin was incubated with **12** or indibulin, the increased tendency of fluorescence intensity was decreased. This result clearly shows that compound **12** exhibited potent tubulin polymerization inhibiting activity, which interestingly displayed a higher potency than indibulin.

3.2.3 | Antimicrotubule effects in HeLa cells

Since tubulin polymerization inhibitors have an effect on microtubule network through interference with microtubule dynamics causing microtubule catastrophe, we performed immunofluorescence staining of α-tubulin in HeLa cells to study the effect of compound **12** on the microtubule network. As shown in Figure 4, the cells without compound exhibited normal filamentous microtubules arrays, with microtubules extending to the peripheral region of the cells, while compound **12** clearly triggered a microtubule catastrophe. From tubulin polymerization and immunofluorescence assay, we conclude that compound **12** is a novel microtubule-depolymerizing agent.

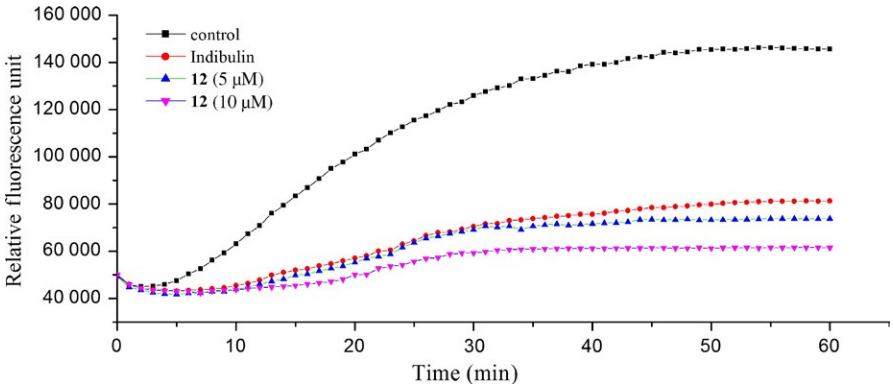

FIGURE 3 Effects of **12** (5, 10 μM) on tubulin polymerization. Indibulin (5 μM) was used as reference drug, 0.1% DMSO as control

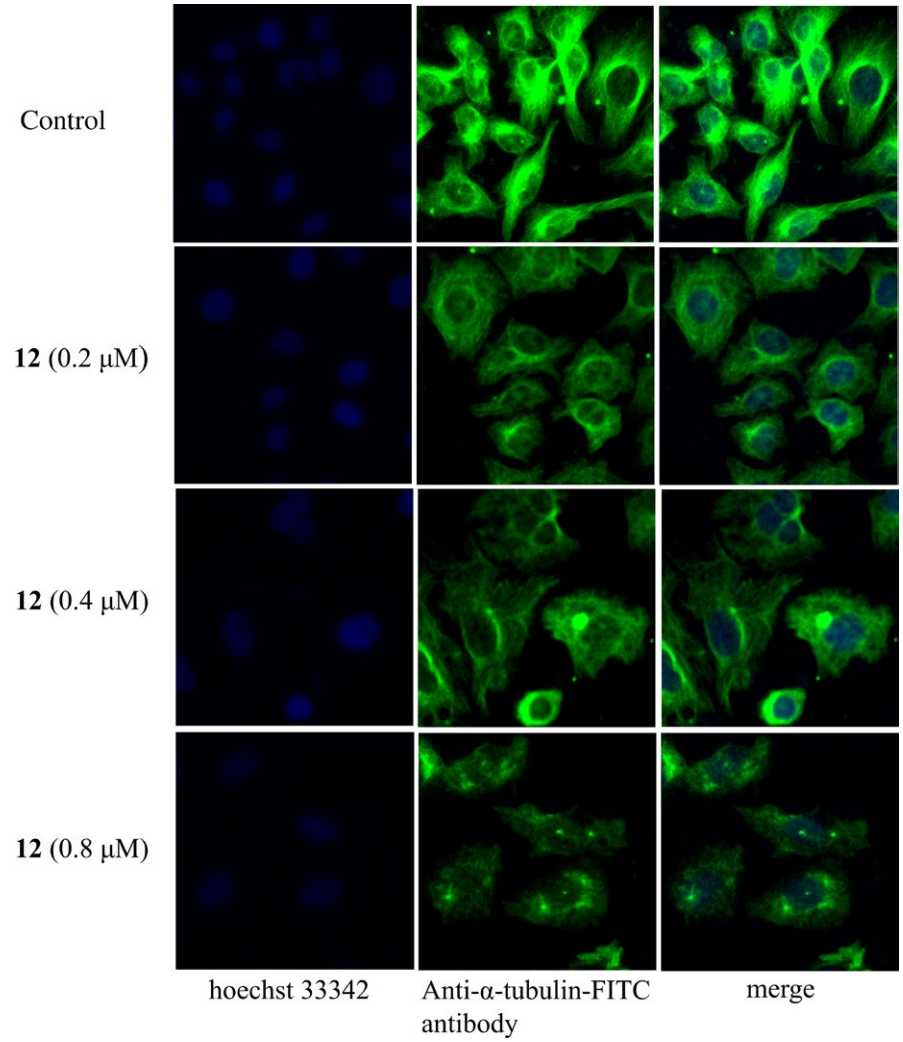

FIGURE 4 Fluorescence microscopic images of HeLa cells stained with Hoechst 33342 or anti-α-tubulin-FITC antibody after treatment with 0.1% DMSO, **12** (0.2, 0.4, 0.8 μM) for 24 hr

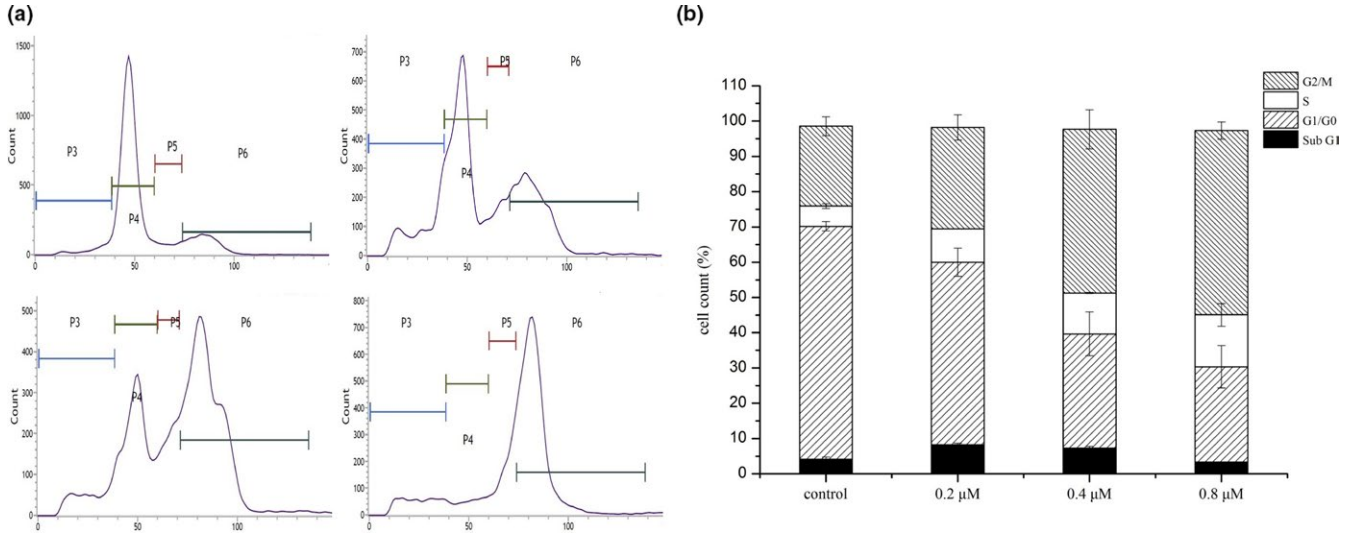

FIGURE 5 (a) Flow cytometry analysis of HeLa cells treated with 0.1% DMSO, 0.2, 0.4, or 0.8 μM compound **12** for 24 hr. (b) The statistical graph of cell cycle distribution

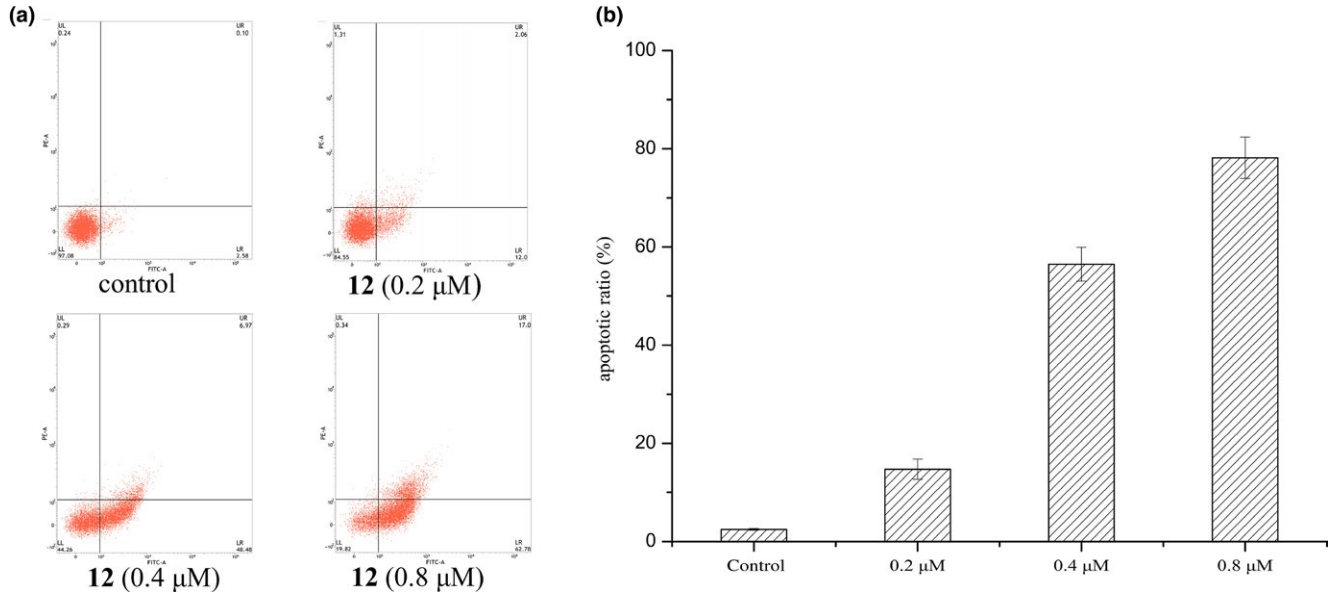

FIGURE 6 (a) Bi-parametric histograms of HeLa cells treated with 0.1% DMSO, 0.2, 0.4, or 0.8 μM compound **12** for 24 hr by flow cytometry after staining (annexin V and PI). (b) Percentage of apoptotic cells

3.2.4 | Cell cycle analysis

Tubulin polymerization inhibitors can interfere with cell division resulting in cell cycle arrest; we next evaluated the cell cycle distribution of compound **12**-treated cells by flow cytometry. As shown in Figure 5, compound **12** induced accumulation of HeLa cells losses in the G1 phase. This suggests that compound **12** induced HeLa cell cycle arrest by affecting cell division. In addition, compound **12** induced an increase in the percentage of cells in the sub-G1 (hypodiploid DNA content peak) phase which may indicate that HeLa cells treated with compound **12** display apoptosis.

3.2.5 | Effects on cell apoptosis progression

The annexin V/propidium iodide (PI) double-staining assay was performed to investigate the effect of compound **12** on cell apoptosis. As shown in Figure 6, the four quadrants represented live cells (annexin V^-/PI^-), early apoptotic cells (annexin V^+/PI^-), late apoptotic cells (annexin V^+/PI^+), and necrotic cells (annexin V^-/PI^+). Compound **12** induced an accumulation of annexin V positive cells in a dose-dependent manner suggested that compound **12** induced apoptosis.

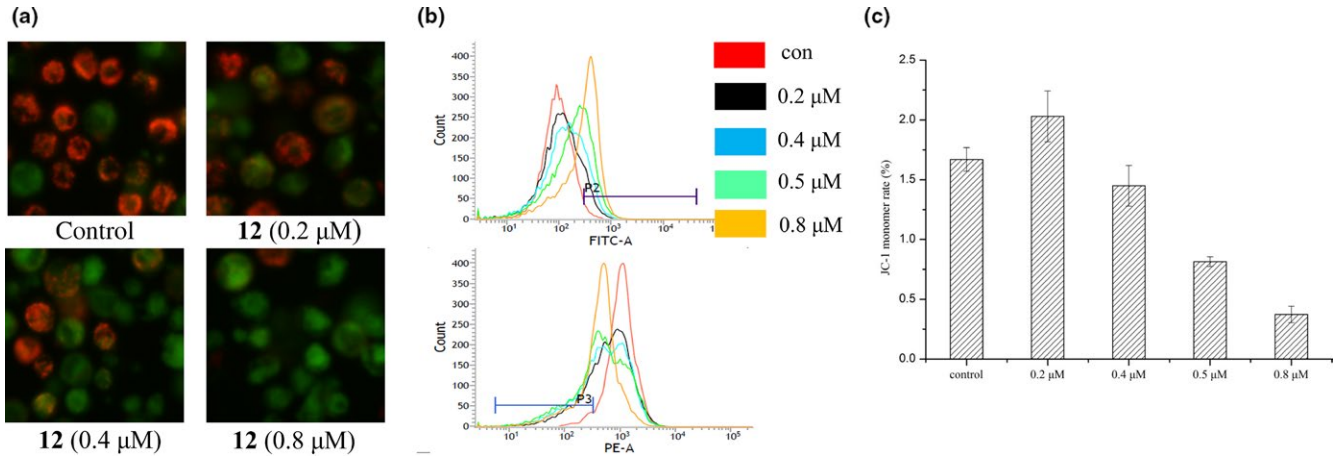

FIGURE 7 (a) Fluorescent images of HeLa cells treated with 0.1% DMSO, 0.2, 0.4, or 0.8 μM compound **12** for 24 hr staining with JC-1. (b) Flow cytometry analysis of HeLa cells. (c) The statistical graph of mitochondrial malfunction cells

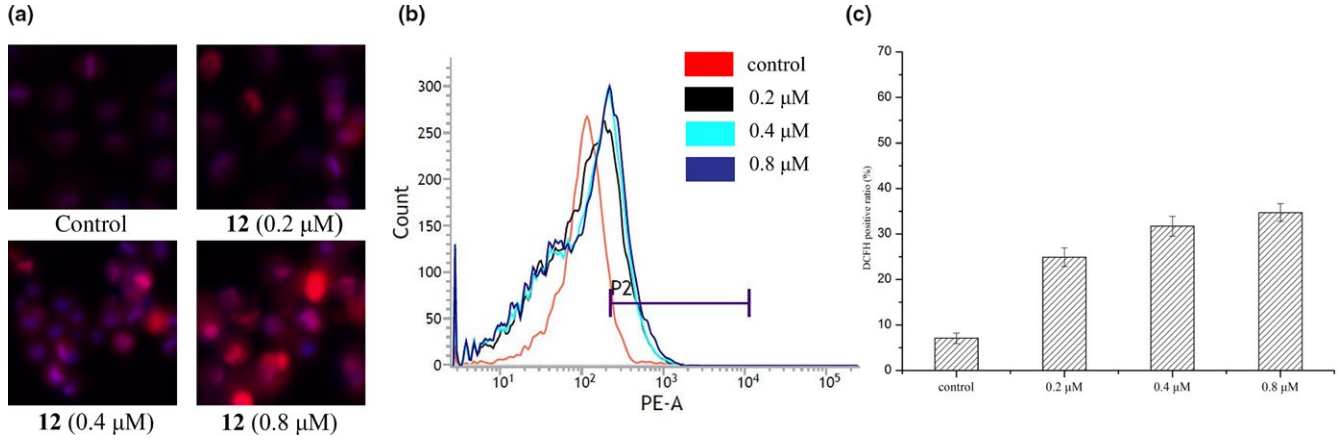

FIGURE 8 (a) Fluorescent images of HeLa cells treated with 0.1% DMSO, 0.2, 0.4, or 0.8 μM compound **12** for 24 hr staining with DHE. (b) Flow cytometry analysis of HeLa cells. (c) The statistical graph of DHE positive ratio

3.2.6 | Effects on mitochondrial membrane potential

Mitochondria play a core role in the mitochondrial-induced apoptosis pathway via changes of the mitochondrial membrane potential. The detection of mitochondrial membrane potential was performed to study whether HeLa cells apoptosis is due to mitochondria malfunction with JC-1 dye being used to detect changes in mitochondrial membrane potential. At high concentration, the dye aggregates which gives a red to orange fluorescence due to high membrane potential. At low concentration, the dye is predominantly a monomer that yields a green fluorescence due to low membrane potential. As shown in Figure 7, a dose-dependent decrease in red fluorescence and an increase in green fluorescence were observed. These results demonstrate that compound **12** induced mitochondrial membrane potential collapse which leads to mitochondrial dysfunction.

3.2.7 | Cellular ROS generation

ROS generation is known to be associated with mitochondrial membrane potential ($\Delta\Psi_m$) changes. The effect of **12** on intracellular ROS level was probed using dihydroethidium (DHE) since it played an important role in anticancer activity. As shown in Figure 8, a significant increase of red fluorescence emission was observed when HeLa cells were treated with compound **12** compared with the control. ROS production induced by compound **12** was dose-dependent which was quantified by flow cytometry. These results indicated that compound **12** increased intracellular ROS levels.

3.2.8 | Effects on expression of G_2/M cell cycle regulatory proteins

The expression of ROS producing-related and cell cycle-related proteins was detected to preliminarily investigate mode of action and pharmacological mechanism. The excessive ROS production could induce G2/M phase cell cycle arrest by modulating the expression of p21 (He et al., 2011). Cells treated with compound **12** resulted in a significant up-regulation of p21 in a time-dependent manner. Chk1, upon activation, phosphorylates Cdc25C at Ser-216 leading to inactivation of cyclin B1/cdc2 (CDK1) complex, which leads to G2/M arrest. As shown in Figure 9, compound **12** induced an up-regulation of Chk1 and affected the expression levels of related proteins.

3.3 | Molecular modeling

To further elucidate the mode of action and to aid in further optimization of the compound, binding mode of compound **12** was computationally evaluated based on the previous work (Qi et al., 2018). To investigate potential binding mode, compound **12** was docked into the colchicine binding site of tubulin (PDB ID: 1SA0) based on our previous study. Some of

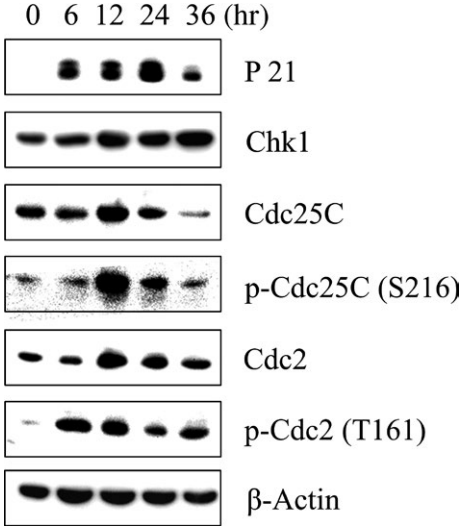

FIGURE 9 Western blot analysis of cell cycle-related protein

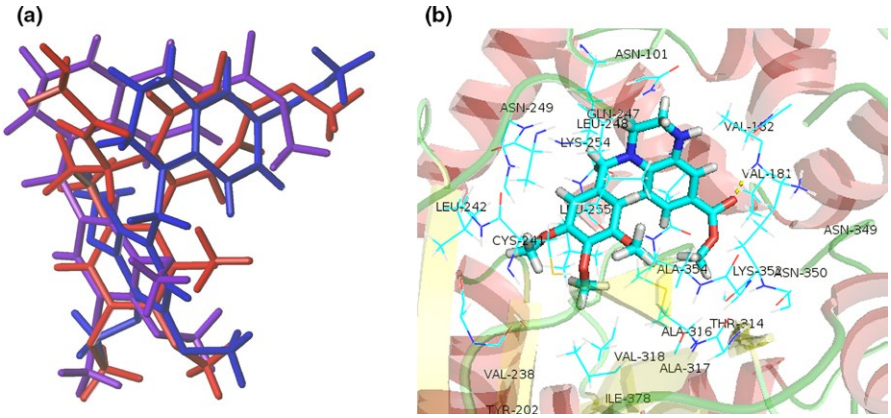

FIGURE 10 (a) Comparison between pose of cocrystallized DAMA-colchicine (red) with tubulin and docking poses of **12**. (b) Proposed binding mode of **12**. Residues within 4 Å of **12** are shown

the higher docking poses ranked by total scores were shown in Figure 10a. The binding orientation of compound **12** was very similar to that of the cocrystallized DAMA-colchicine. As shown in Figure 10b, a hydrogen bond is present between compound **12** and VaL 181 in the loop of α-tubulin. The trimethoxyphenyl moiety made nonpolar interaction with Cys 241, Leu 242, Leu248, Val 318, and Ile 378 of β-tubulin.

4 | CONCLUSIONS

We have synthesized a series of quinoxaline derivatives that were evaluated for antiproliferative activity against human cancer cell lines (Hela, SMMC-7721, HT29). Among these compounds, Compound **12** exhibited potent cytotoxicity with IC_{50} ranging from 0.19 to 0.51 μM. Compound **12** inhibited the tubulin polymerization and induced cell cycle arrest at G2/M phase. Further, compound **12** induced an increase of intracellular ROS levels. Compound **12** also led to cancer cells apoptosis via mitochondrial pathway. The Western blot analysis showed that compound **12** induced up-regulation of p21 and affected the expression of cell cycle-related proteins. This work provided new agents for the development of the promising anticancer drugs. Optimization and structure–activity relationship (SAR) studies are currently underway and will be reported in due course. Furthermore, we are actively investigating the mechanism of action, which will give more insight into the biological activity observed.

ACKNOWLEDGMENTS

The authors are grateful for the financial support from Program for Science Technology Innovation Talents in Universities of Henan Province (16HASTIT029) and the National Natural Science Foundation of China (No. 21272056). In addition, this work was also supported by National Natural Science Foundation of China (No. U1704176, No. U1404819), Key Scientific Research Program of the Higher Education Institutions of Henan Province (Grant No. 15A350005), and Research Fund of Henan University (2015YBZR043).

CONFLICT OF INTEREST

The authors declare that there are no conflicts of interests.

ORCID

Jianguo Qi https://orcid.org/0000-0002-8087-1169

REFERENCES

Ajani, O. O. (2014). Present status of qunioxaline motifs: Eecellent pathfinders in therapeutic medicine. *European Journal of Medicinal Chemistry*, *85*, 688–715. https://doi.org/10.1016/j.ejmech.2014.08.034

Asby, D. J., Radigois, M. G., Wilson, D. C., Cuda, F., Chai, C. L., Chen, A., … Tavassoli, A. (2016). Triggering apoptosis in cancer cells with an analogue of cribrostatin 6 that elevates intracellular ROS. *Organic & Biomolecular Chemistry*, *14*, 9322–9330. https://doi.org/10.1039/C6OB01591C

Bacher, G., Nickel, B., Emig, P., Vanhoefer, U., Seeber, S., Shandra, A., … Beckers, T. (2001). D-24851, a novel synthetic microtubule inhibitor, exerts curative antitumoral activity in vivo, shows efficacy toward multidrug-resistant tumor cells, and lacks neurotoxicity. *Cancer Research*, *61*, 392–399.

Banerjee, S., Arnst, K. E., Wang, Y., Kumar, G., Deng, S., Yang, L., … Miller, D. D. (2018). Heterocyclic-fused pyrimidines as novel tubulin polymerization inhibitors targeting the colchine binding site: Structural basis and antitumor efficacy. *Journal of Medicinal Chemistry*, *61*, 1704–1718. https://doi.org/10.1021/acs.jmedchem.7b01858

Bhalla, K. N. (2003). Microtubule-targeted anticancer agents and apoptosis. *Oncogene*, *22*, 9075–9086. https://doi.org/10.1038/sj.onc.1207233

Bueno, O., Tobajas, G., Quesada, E., Estévez-Gallego, J., Noppen, S., Camarasa, M. J., … Pérez-Pérez, M. J. (2018). Conformational mimetics of the α- methyl chalcone TUB091 binding tubulin: Design, synthesis and antiproliferative activity. *European Journal of Medicinal Chemistry*, *148*, 337–348. https://doi.org/10.1016/j.ejmech.2018.02.019

Cui, M. T., Jiang, L., Goto, M., Hsu, P. L., Li, L., Zhang, Q., … Xie, L. (2017). In vivo and mechanistic studies on antitumor lead 7-m ethoxy-4-(2-methylquinazolin-4-yl)-3,4-dihydroquinoxalin- 2(1*H*)-one and its modification as a novel class of tubulin-binding tumor-vascular disrupting agents. *Journal of Medicinal Chemistry*, *60*, 5586–5598. https://doi.org/10.1021/acs.jmedchem.7b00273

Diana, P., Martorana, A., Barraja, P., Montalbano, A., Dattolo, G., Cirrincione, G., … Viola, G. (2008). Isoindolo[2,1-a]quinoxaline derivatives, novel potent antitumor agents with dual inhibition of tubulin polymerization and topoisomerase I. *Journal of Medicinal Chemistry*, *51*, 2387–2399. https://doi.org/10.1021/jm070834t

Dohle, W., Jourdan, F. L., Menchon, G., Prota, A. E., Foster, P. A., Mannion, P., … Potter, B. V. L. (2018). Quinazolinone-based anticancer agents: Synthesis, antiproliferative SAR, antitubulin activity, and tubulin co-crystal structure. *Journal of Medicinal Chemistry*, *61*, 1031–1044. https://doi.org/10.1021/acs.jmedchem.7b01474

Du, J., Li, B., Fang, Y., Liu, Y., Wang, Y., Li, J., … Wang, X. (2015). Overexpression of class III β-tubulin, sox 2, and nuclear survivin is predictive of taxane resistance in patients with stage III ovarian epithelial cancer. *BMC Cancer*, *15*, 536–546. https://doi.org/10.1186/s12885-015-1553-x

Dumontet, C., & Jordan, M. A. (2010). Microtubule-binding agents: A dynamic field of cancer therapeutics. *Nature Reviews. Drug Discovery*, *9*, 790–803. https://doi.org/10.1038/nrd3253

Gangjee, A., Zhao, Y., Lin, L., Raghavan, S., Roberts, E. G., Risinger, A. L., … Mooberry, S. L. (2010). Synthesis and discovery of water-soluble microtubule targeting agents that bind to the colchicine site on tubulin and circumvent Pgp mediated resistance. *Journal of Medicinal Chemistry*, *53*, 8116–8128. https://doi.org/10.1021/jm101010n

Gigant, B., Wang, C., Ravelli, R. B., Roussi, F., Steinmetz, M. O., Curmi, P. A., … Knossow, M. (2005). Structural basis for the regulation of tubulin by vinblastine. *Nature*, *435*, 519–522. https://doi.org/10.1038/nature03566

He, L., Nan, M. H., Oh, H. C., Kim, Y. H., Jang, J. H., Erikson, R. L., … Kim, B. Y. (2011). Asperlin induces G2/M arrest through ROS generation and ATM pathway in human cervical carcinoma cells. *Biochemical and Biophysical Research Communications*, *409*, 489–493. https://doi.org/10.1016/j.bbrc.2011.05.032

Hirota, K., Murata, M., Sachi, Y., Nakamura, H., Takeuchi, J., Mori, K., & Yodoi, J. (1999). Distinct roles of thioredoxin in the cytoplasm and in the nucleus. A two-step mechanism of redox regulation of transcription factor NF-kappa B. *Journal of Biological Chemistry*, *274*, 27891–27897. https://doi.org/10.1074/jbc.274.39.27891

Huang, P., Feng, L., Oldham, A. E., Keating, J. M., & Plunkett, W. (2000). Superoxide dismutase as a target for the selective killing of cancer cells. *Nature*, *407*, 390–395. https://doi.org/10.1038/35030140

Jordan, M. A., & Wilson, L. (2004). Microtubules as a target for anticancer drugs. *Nature Reviews Cancer*, *4*, 253–265. https://doi.org/10.1038/nrc1317

Kavallaris, M. (2010). Microtubules and resistance to tubulin-binding agents. *Nature Reviews Cancer*, *10*, 194–204. https://doi.org/10.1038/nrc2803

Lauria, A., Gentile, C., Mingoia, F., Palumbo Piccionello, A., Bartolotta, R., Delisi, R., … Martorana, A. (2018). Design, synthesis, and biological evaluation of a new class of benzo[b]furan derivatives as antiproliferative agents, with in silico predicted antitubulin activity. *Chemical Biology & Drug Design*, *91*, 39–49. https://doi.org/10.1111/cbdd.13052

Lecane, P. S., Karaman, M. W., Sirisawad, M., Naumovski, L., Miller, R. A., Hacia, J. G., & Magda, D. (2005). Motexafin gadolinium and zinc induce oxidative stress responses and apoptosis in B-cell lymphoma lines. *Cancer Research*, *65*, 11676–11688. https://doi.org/10.1158/0008-5472.CAN-05-2754

Li, L., Jiang, S., Li, X., Liu, Y., Su, J., & Chen, J. (2018). Recent advances in trimethoxyphenyl (TMP) based tubulin inhibitors targeting the colchicine binding site. *European Journal of Medicinal Chemistry*, *151*, 8–20.

Lu, Y., Chen, J., Xiao, M., Li, W., & Miller, D. D. (2012). An overview of tubulin inhibitors that interact with the colchicine binding site. *Pharmaceutical Research*, *29*, 2943–2971. https://doi.org/10.1007/s11095-012-0828-z

Ohsumi, K., Nakagawa, R., Fukuda, Y., Hatanaka, T., Morinaga, Y., Nihei, Y., … Tsuji, T. (1998). Novel combretastatin analogues effective against murine solid tumors: Design and structure-activity relationships. *Journal of Medicinal Chemistry*, *41*, 3022–3032. https://doi.org/10.1021/jm980101w

Pang, Y., An, B., Lou, L., Zhang, J., Yan, J., Huang, L., … Yin, S. (2017). Design, synthesis, and biological evaluation of novel selenium-containing isocombrestatins and phenstatins as antibumor agents. *Journal of Medicinal Chemistry*, *60*, 7300–7314. https://doi.org/10.1021/acs.jmedchem.7b00480

Perez, E. A. (2009). Microtubule inhibitors: Differentiating tubulin-inhibiting agents based on mechanisms of action, clinical activity, and resistance. *Molecular Cancer Therapeutics*, *8*, 2086–2095. https://doi.org/10.1158/1535-7163.MCT-09-0366

Pérez-Melero, C., Maya, A. B., del Rey, B., Peláez, R., Caballero, E., & Medarde, M. (2004). A new family of quinoline and quinoxaline analogues of combretastatins. *Bioorganic & Medicinal Chemistry Letters*, *14*, 3771–3774. https://doi.org/10.1016/j.bmcl.2004.04.098

Qi, J., Dong, H., Huang, J., Zhang, S., Niu, L., Zhang, Y., & Wang, J. (2018). Synthesis and biological evaluation of *N*-substituted 3-oxo-1,2,3,4-tetrahydro-quinoxaline-6-carboxylic acid derivatives as tubulin polymerization inhibitors. *European Journal of Medicinal Chemistry*, *143*, 8–20. https://doi.org/10.1016/j.ejmech.2017.08.018

Raj, L., Ide, T., Gurkar, A. U., Foley, M., Schenone, M., Li, X., … Lee, S. W. (2011). Selective killing of cancer cells by a small molecule targeting the stress response to ROS. *Nature*, *475*, 231–234. https://doi.org/10.1038/nature10167

Stanton, R. A., Gernert, K. M., Nettles, J. H., & Aneja, R. (2011). Durgs that target dynamic microtubules: A new molecular perspective. *Medicinal Research Reviews*, *31*, 443–481. https://doi.org/10.1002/med.20242

Suman, P., Murthy, T. R., Rajkumar, K., Srikanth, D., Dayakar, C. H., Kishor, C., … Raju, B. C. (2015). Synthesis and structure-activity relationships of pyridinyl-1H-1,2,3-triazolyldihydroisoxazoles as potent inhibitors of tubulin polymerization. *European Journal of Medicinal Chemistry*, *90*, 603–619. https://doi.org/10.1016/j.ejmech.2014.11.063

Szatrowski, P. T., & Nathan, F. C. (1991). Production of large amounts of hydrogen peroxide by human tumor cells. *Cancer Research*, *51*, 794–798.

Tariq, S., Somakala, K., & Amir, M. (2018). Quinoxaline: An insight into the recent pharmacological advances. *European Journal of Medicinal Chemistry*, *143*, 542–557. https://doi.org/10.1016/j.ejmech.2017.11.064

Wang, J., Chen, J., Miller, D. D., & Li, W. (2014). Synergistic combination of novel tubulin inhibitor ABI-274 and vemurafenib overcomes vemurafenib acquired resistance in $BRAF^{V600E}$ melanoma. *Molecular Cancer Therapeutics*, *13*, 16–26. https://doi.org/10.1158/1535-7163.MCT-13-0212

Wang, Z., Chen, J., Wang, J., Ahn, S., Li, C. M., Lu, Y., … Li, W. (2012). Novel tubulin polymerization inhibitors overcome multidrug resistance and reduce melanoma lung. *Pharmaceutical Research*, *29*, 3040–3052. https://doi.org/10.1007/s11095-012-0726-4

How to cite this article: Qi J, Huang J, Zhou X, et al. Synthesis and biological evaluation of quinoxaline derivatives as tubulin polymerization inhibitors that elevate intracellular ROS and triggers apoptosis via mitochondrial pathway. *Chem Biol Drug Des*. 2019;00:1–11. https://doi.org/10.1111/cbdd.13459

SUPPORTING INFORMATION

Additional supporting information may be found online in the Supporting Information section at the end of the article.